Journal of Luminescence 199 (2018) 258–265

Contents lists available at ScienceDirect

Journal of Luminescence

journal homepage: www.elsevier.com/locate/jlumin

# Effect of pH on Eosin Y/PAMAM interactions studied from absorption spectroscopy and molecular dynamics simulations

Luis F. Barraza[a], Matías Zuñiga[a], Joel B. Alderete[b], Ernesto M. Arbeloa[c,d,*], Verónica A. Jiménez[a,**]

[a] Departamento de Ciencias Químicas, Facultad de Ciencias Exactas, Universidad Andres Bello, Sede Concepción, Autopista Concepción-Talcahuano 7100, Talcahuano, Chile
[b] Departamento de Química Orgánica, Facultad de Ciencias Químicas, Universidad de Concepción, Casilla 160-C, Concepción 4070371, Chile
[c] Universidad Nacional de Río Cuarto, Río Cuarto, 5800 Córdoba, Argentina
[d] Consejo Nacional de Investigaciones Científicas y Técnicas (CONICET), Argentina

ARTICLE INFO

*Keywords:*
Dendrimers
Eosin Y
Molecular dynamics
PAMAM
Host-guest chemistry

ABSTRACT

Absorption spectroscopy experiments were carried out to examine the 1:1 supramolecular interaction between Eosin Y (EOS) and low generation G0-G3 poly(amido amine) (PAMAM) dendrimers at neutral and basic media, aimed at gaining insight about the role of pH and dendrimer generation on EOS-PAMAM binding. Our results revealed that EOS complexation is favored under neutral pH conditions, and that the supramolecular interaction strengthens as the dendrimer generation increases. Further molecular-level information regarding EOS-PAMAM systems was obtained from Molecular Dynamics (MD) simulations, Non-Covalent Interaction (NCI) analysis and MM/PBSA binding free energy calculations, which were carried out to examine the role of the generation, charge, and protonation state of PAMAM on the structure, conformation, and preferable interactions with EOS at neutral and basic pH conditions. Theoretical predictions were in high agreement with experimental results, showing that neutral pH allows a faster, deeper, and more stable complexation of the dye within dendrimer cavities, and that higher generation dendrimers induce a larger affinity towards EOS. According to MD results, the binding mode of the dye favors the interaction of the xanthene moiety within internal dendrimer cavities through the establishment of attractive van der Waals contacts. On the other hand, the carboxylate moiety interacts with the outermost dendrimer branches and remains exposed towards the solvent in G0-G2 PAMAM. These results support the validity of using MD simulations as auxiliary tools to deal with supramolecular complexation phenomena involving PAMAM dendrimers as host molecules.

## 1. Introduction

Eosin Y (EOS) is a well-known xanthene fluorescent dye with a wide range of biomedical and photochemical applications due to its high light absorption in the visible region and high fluorescence quantum yield (Fig. 1) [1–5] Over the years, EOS has been extensively employed in cell staining, as a pH indicator, as a dye pigment, and as an organic visible light photocatalyst in synthetic transformations. [6] The use of EOS and other metal-free fluorescent dyes in photoredox reactions has attracted great attention due to their advantageous properties compared to organometallic dyes, such as lower price, reduced toxicity, outperformance, and higher environmental compatibility. Upon excitation by visible light, EOS undergoes a rapid intersystem crossing to the lowest energy triplet state, after which it becomes more oxidizing and more reducing than its ground state. [6] The photocatalytic behavior of EOS can be modulated by charge transfer to the photoexcited state, either through covalent conjugation or supramolecular association with molecular nanostructures acting as electron donors, which can be exploited for a variety of purposes such as chemosensors, photon energy transfer, imaging, and photopolymerization, among others. Within suitable molecular systems for EOS encapsulation, the use of dendritic polymers is of major importance, since these entities offer a unique molecular scaffold to create very well-defined nanostructures with versatile purposes. [7,8]

Dendrimers have a highly precise core-shell architecture in which repetitive branches emerge from a central core in a layer-by-layer fashion, leading to branched symmetric nanostructures of increasing generation. Commercially available poly(amido amine) (PAMAM)

* Corresponding author at: Universidad Nacional de Río Cuarto, Río Cuarto, 5800 Córdoba, Argentina.
** Corresponding author.
*E-mail addresses:* earbeloa@exa.unrc.edu.ar (E.M. Arbeloa), veronica.jimenez@unab.cl (V.A. Jiménez).

https://doi.org/10.1016/j.jlumin.2018.03.068
Received 7 November 2017; Received in revised form 4 January 2018; Accepted 23 March 2018
Available online 24 March 2018

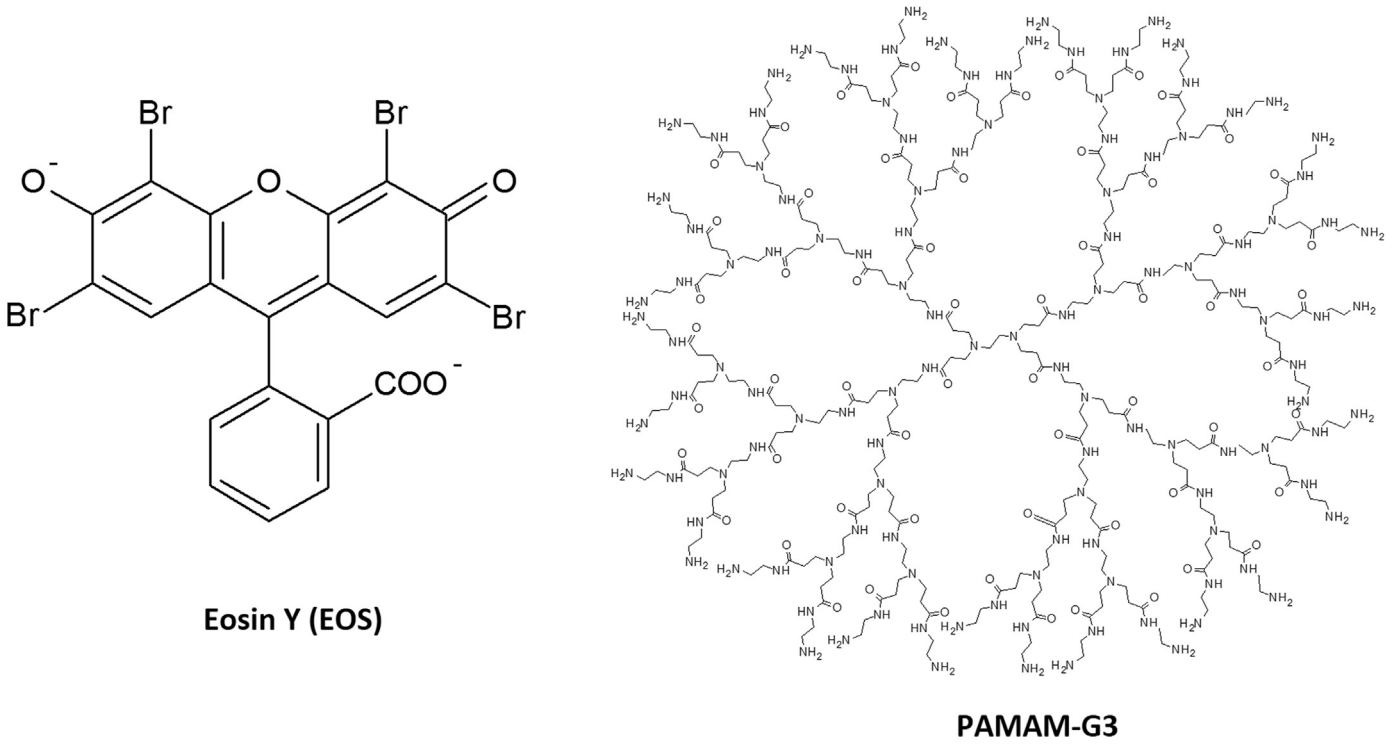


**Fig. 1.** Structure of PAMAM-G3 dendrimer and Eosin Y (EOS) dye molecule in its dianionic form.

dendrimers are the most common and widely employed class of dendritic polymers (Fig. 1). [9] PAMAM dendrimers are water-soluble polymers consisting of an alkyl-diamine core, tertiary amine branches and polar primary amine surface groups, which confer PAMAM with a high versatility for chemical modification. In aqueous solution, the total charge of PAMAM varies at different pH conditions as the surface amino groups (pKa 9.4–9.7) and internal tertiary amino moieties (pKa 3.9) [10] adopt different protonation states, affecting the size, conformation and encapsulation capability of the polymer. Thus, at neutral pH the amino-functional PAMAM surface is cationic and the dendrimer moiety adopts an extended structure, whereas in basic conditions (pH > 9) the dendrimer surface becomes neutral and the macromolecule is more compact. Regarding to tertiary amines, these groups are protonated under strong acidic conditions (pH < 3.9) leading to a more expanded dendrimer conformation. In the past years, PAMAM dendrimers have been assayed as supramolecular hosts for EOS encapsulation showing promissory results for their use as soluble macrophotoinitiators of polymerization reactions with low ecological impact. [11] In recent reports, Arbeloa *et al.* studied the photophysics of EOS in the presence of low generation (G0-G3) PAMAM dendrimers in alkaline aqueous solution by stationary and time-resolved spectroscopy, showing that the EOS-PAMAM binding constant increases as the dendrimer generation becomes higher, and that the electron transfer from PAMAM to EOS is a highly favored process. [7,8] Despite the valuable potential of the EOS-PAMAM systems, little information has been collected regarding the nature of the dye-dendrimer supramolecular association or the factors ruling this interaction. Particularly, considering that EOS is a diprotic weak acid itself, studying the role of pH on the structure and strength of EOS-PAMAM interactions is a relevant subject to address, aimed at identifying environmental conditions that can modulate the photochemical properties of EOS for future photocatalytic applications.

In this work, EOS-PAMAM interactions at neutral and basic pH conditions were examined through a combination of computational and experimental methods comprising absorption spectroscopy, fully-atomistic molecular dynamics (MD) simulations, Non-Covalent Interaction (NCI) analysis and MM/PBSA binding free energy calculations, with the aim of gaining insight into the structure, binding properties and driving forces behind the encapsulation of EOS molecules with G0-G3 PAMAM dendrimers in different protonation states. Theoretical predictions were compared to experimental results concerning the association of EOS with G0-G3 PAMAM dendrimers at neutral and basic pH conditions measured from absorption spectroscopy, showing a high level of agreement.

## 2. Material and methods

### 2.1. Absorption spectroscopy experiments

EOS and G0-G3 PAMAM dendrimers with ethylenediamine core in methanol solution (20%) were purchased from Aldrich, St. Louis, MO, USA and used without further purification. Dendrimers solutions were properly diluted with HPLC grade methanol (Sintorgan) as necessary. Aqueous solutions at pH 7 were prepared with bi-distilled water and a $KH_2PO_4$/NaOH buffer, both reagents of analytical grade. Absorption spectra were recorded on a Hewlett Packard 6453E diode array spectrophotometer, No changes in the absorption spectra of EOS were recorded in the 7–10 pH range. Therefore, concentrations of the EOS aqueous solutions (4 μM) were determined from absorption spectra (Abs ca. 0.4 at 517 nm) and the absorptivity-molar coefficient (91,000 $M^{-1}$ $cm^{-1}$ at 517 nm, Ref. [8]). Throughout all experiments the addition of dendrimers was performed using microsyringes under constant stirring, such that the methanol content in the Eos solutions was < 5%. There were no changes in the spectra by this additional methanol, as verified through blank tests. All data were properly corrected by dilution effects. The measurements were performed at least by duplicate.

### 2.2. Molecular dynamics simulations

The initial coordinates for G0-G3 PAMAM dendrimers were generated using the well-tested Dendrimer Builder Toolkit (DBT) software [12], using the implementations of the AMBER 16 software, and the General AMBER Force Field (GAFF) parameters. [13] Different protonation states of the surface amino groups of PAMAM were considered

aimed at emulating neutral (pH 7.0) and alkaline (pH 10) conditions. [10] At neutral pH, the primary amine groups of PAMAM are protonated, whereas under alkaline conditions the primary amines remain neutral. The initial structure of EOS was obtained from ab initio calculations at the B3LYP/6-31 + G(d,p) level using the Gaussian 09 software, [14] considering the dianionic deprotonated form of their phenolic and carboxyl groups ($pK_{a1OH}$ 2.02 and $pK_{a2COOH}$ 3.8). [15] The Gaussian output file was then used to derive partial atomic charges using the Antechamber module implemented in AMBERTOOLS 16 and the parameters of the GAFF force field. The GAFF atom types and RESP atomic charges of EOS molecule are given in Supplementary material (Fig. S1 and Table S1). Initial structures of EOS complexes with G0-G3 PAMAM dendrimers at neutral and alkaline pH conditions were built by placing one EOS unit at 13 Å from the surface of a pre-equilibrated dendrimer moiety, which was extracted from previous unrestricted 100 ns MD runs. In these initial structures, the dye was located far away from the dendrimer structure, thus describing a non-complexed state for EOS-PAMAM systems. All systems were built considering a 1:1 stoichiometry, aimed at mimicking the experimental dye:dendrimer ratio determined by Arbeloa et al. [8]. Additionally, the appropriate number of chloride (Cl-) or sodium (Na+) counterions were randomly added to each system to maintain charge neutrality. Systems were solvated with explicit TIP3P water in a cubic water box with a solvation layer of 12 Å from the EOS-PAMAM system. Initial structures and details about the simulated systems are provided as Supplementary material (Table S1). Solvated structures were minimized in two sequential steps: (i) in the first step the atomic positions of PAMAM and EOS were fixed using a strong harmonic restraint with a force constant of 500 (kcal/mol)/$Å^2$, and water and counterions were minimized using 1000 steps of steepest descent and 2000 steps of conjugate gradient methods, (ii) in the second step all restrains were released and the entire system was subjected to 1000 steps of steepest descent and 2000 steps of conjugate gradient minimization methods. Minimized systems were progressively heated from 0 to 300 K without any restrain for 1000 ps in the canonical ensemble (NVT), followed by 2000 ps of equilibration dynamics performed at 300 K using the NVT ensemble employing a time step of 1 fs, after which the formation and stabilization of EOS-PAMAM complexes was corroborated. Finally, 100 ns of unconstrained production runs were carried out using the isobaric-isothermal ensemble (NPT) at 300 K and 1 atm with a time step of 2 fs. Constant temperature was imposed employing a Langevin dynamics approach with a collision frequency of 1 $ps^{-1}$, whereas constant pressure was fixed using the Langevin Thermostat. Long-range electrostatic interactions were evaluated with the standard Particle-Mesh Ewald (PME) method [16], using periodic boundary conditions. For non-bonded calculations a cutoff of 10 Å was fixed, whereas all bonds involving hydrogen atoms were kept rigid using the SHAKE constraint algorithm. [17]

### 2.3. Trajectory analysis

Trajectory analysis was performed using the VMD software utilities [17] and the CPPTRAJ module implemented in Amber16 software. Equilibration of the systems under study was evaluated from RMSD calculations. The radius of gyration (*Rg*) was evaluated to assess the size of PAMAM under different pH conditions. The shape of free and complexed dendrimers was evaluated from the calculation of the aspect ratio (Ix/Iy and Ix/Iz) and asphericity (δ) along the MD trajectory. The complexation process along the trajectory was evaluated following the time evolution of the separation distance between center of mass of dendrimer cores and EOS molecules, while the relative location of EOS molecules within PAMAM macrostructure was evaluated using radial distribution functions (RDF). To obtain a visual description of the relative contribution of weak intermolecular interactions (i.e. hydrogen bonds, van der Waals interactions, and steric clashes) in the stabilization of EOS-PAMAM complexes, non-covalent interaction (NCI) analysis was carried out using the Multiwfn[1] software, using the last frame of the corresponding MD trajectories. The number of the grids in the cube was set to 250 × 250 × 250 Å, with a 0.1 Å step size along x, y, and z coordinates. The visual representations and colors of averaged weak interactions and NCI indices were obtained using VMD software.

The strength of EOS-PAMAM interactions at neutral and alkaline conditions was evaluated from MM/PBSA calculations using the MMPBSA.py python utility provided in the Amber16 software under a single trajectory approach. Binding free energy calculation were estimated from 250 snapshots retrieved from the last 50 ns of each MD run, considering an ionic strength of 0.1 mM and nonpolar optimization method inp = 2. Dielectric constants for the solvent and the system were set to 80 and 1, respectively. The entropic contribution to the binding free energy was neglected due to computational costs.

## 3. Results

In this report, absorption spectroscopy experiments were carried out to examine the supramolecular association between EOS and PAMAM dendrimers of G0-G3 generation under neutral conditions. These results are complementary to those obtained in our previous report, in which the EOS-PAMAM association was studied at basic pH medium [7,8]. The main goal of the present study is to gain insight about the role of pH and dendrimer generation on the stability of EOS-PAMAM supramolecular systems. Additionally, fully atomistic MD simulations of EOS-PAMAM complexes were employed to provide a molecular level understanding about the factors that govern the supramolecular association of the dye with G0-G3 PAMAM dendrimers at neutral and basic pH, considering two protonation states for the surface amino groups of the dendritic moieties. At neutral pH, terminal amino groups of PAMAM were simulated in their protonated state ($-NH_3^+$), whereas at basic pH these groups were considered in their neutral form ($-NH_2$). In the case of EOS, this molecule was simulated considering its dianionic deprotonated form at both neutral and basic conditions, as the $pK_a$ of the phenolic and carboxyl moieties are 2.0 and 3.8, respectively.

### 3.1. Absorption spectroscopy

Absorption spectroscopy experiments were carried out to determine the binding constants ($K_{bind}$) and binding free energies ($\Delta G_{bind}$) for the supramolecular interaction between EOS and G0-G3 PAMAM dendrimers at neutral pH. Experiments were carried out considering increasing dendrimer concentrations as described in our previous work. [8] The dye registered a maximum absorption at 517 nm and exhibited changes in the position and intensity of its main spectral band in the presence of PAMAM, which can be attributed to the complexation of the dye into the less polar environment provided by dendrimer branches (Fig. 2). A progressive bathochromic shift becomes more evident in higher generation dendrimers, indicating that EOS-PAMAM interaction is size-dependent. The corresponding $K_{bind}$ values for EOS-PAMAM systems were determined considering a simple equilibrium model for a 1:1 stoichiometry, as reported in our previous report. The validity of this assumption is based on the fact that dendrimer concentration was at least 200-fold higher than the dye concentration, which makes unsuitable having a different complex stoichiometry. Under this approach, the $K_{bind}$ are estimated from absorbance measurements using the linearized Eq. (1):

$$\frac{1}{\Delta A} = \frac{1}{[EOS]K_{bind}\Delta\varepsilon[PAMAM]} + \frac{1}{[EOS]\Delta\varepsilon} \quad (1)$$

where ΔA is the absorbance change experienced by the dye at different PAMAM concentrations, and $\Delta\varepsilon$ is the difference in the extinction coefficients between free and complexed dye molecules. $K_{bind}$ and estimated $\Delta G_{bind}$ (kcal $mol^{-1}$) for EOS-PAMAM systems at neutral pH are reported in Table 1, together with our previous findings regarding $K_{bind}$ values for EOS-PAMAM systems at basic pH [8]. Linearized data is

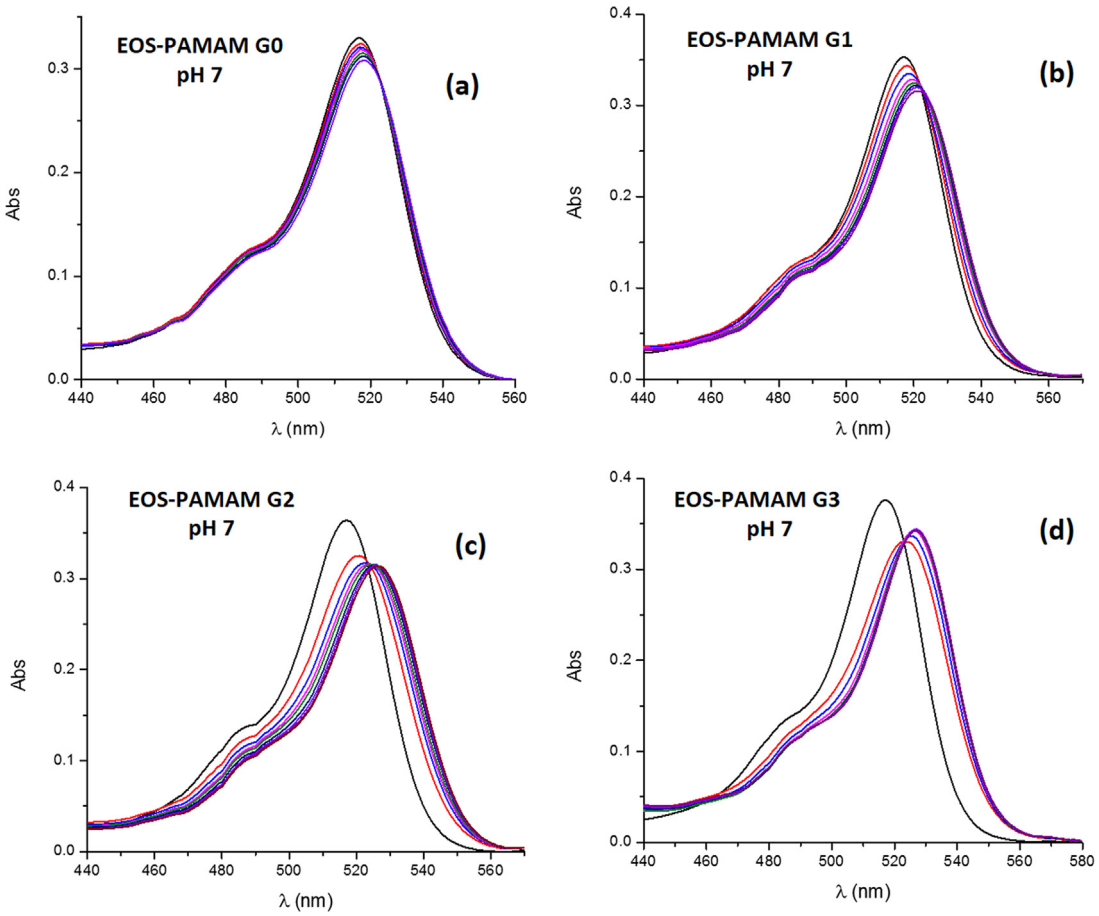


**Fig. 2.** Absorption spectra of EOS in neutral aqueous solution in the absence, and in the presence of increasing concentrations of PAMAM dendrimers: (a) 0.41–4.8 mM of G0; (b) 0.14–1.7 mM of G1; (c) 0.07–0.77 mM of G2; and (d) 0.03–0.36 mM of G3. The concentration of PAMAM increases from left to right.

**Table 1**
Experimental binding constants $K_{bind}$ and binding free energies $\Delta G_{bind}$ (kcal mol$^{-1}$) for the interaction between EOS and low generation G0-G3 PAMAM dendrimers at neutral and basic pH conditions obtained from absorption spectroscopy.

| pH | System | $K_b$ ($M^{-1}$)[b] | $\Delta G_{bind}$ (kcal mol$^{-1}$) |
|---|---|---|---|
| Neutral | G0-EOS | 400 | −3.5 |
| | G1-EOS | 2000 | −4.5 |
| | G2-EOS | 11,000 | −5.5 |
| | G3-EOS | 70,000 | −6.6 |
| Basic | G0-EOS | 50[a] | −2.3[a] |
| | G1-EOS | 780[a] | −3.9[a] |
| | G2-EOS | 5800[a] | −5.1[a] |
| | G3-EOS | 12,900[a] | −5.6[a] |

[a] Data was retrieved from the work of Arbeloa et al. [8].
[b] Estimated error ± 10%.

supplied as Supplementary material. Our results revealed that the EOS-PAMAM association is strongly favored at neutral pH conditions, which can be attributed to a more favorable interaction between EOS and the protonated surface amino groups of PAMAM under neutral pH over basic medium, thus supporting an external complexation mechanism of an electrostatic nature. Nevertheless, the stronger changes observed in the intensity and position of the absorption band of EOS in the presence of G2 and G3 also evidence a deeper penetration of the dye within dendrimer branches, which can be a consequence of an internal mechanism of complexation. To further elucidate the structure the preferable interaction sites for EOS-PAMAM systems, and to provide insight into the molecular features responsible for the increased affinity of EOS towards PAMAM complexation in a neutral pH medium, fully atomistic MD simulations were carried out as detailed in the following section.

### 3.2. Molecular dynamics simulations

Fully atomistic MD simulations of EOS-PAMAM supramolecular systems in a 1:1 ratio were carried out aimed at increasing understanding about the structure and stability of these supramolecular systems at neutral and basic pH. 100 ns of unconstrained NPT molecular dynamics were run for each EOS-PAMAM system, considering G0-G3 dendrimer generations and two protonation states, as early described. Structural parameters as the radius of gyration ($R_g$), aspect ratio ($I_x/I_y$ and $I_x/I_z$), and asphericity (δ) of PAMAM dendrimers and EOS-PAMAM complexes were evaluated from MD simulations in the search for variations in the dendrimer shape upon ligand complexation (Table 2). The plots corresponding to the time evolution of these structural parameters are provided as Supplementary material, and reveal the stability of the simulated systems along the MD run.

The radius of gyration ($R_g$) is a measure of the size of a molecular system and is defined as

$$\langle R_g^2 \rangle = \frac{1}{M} \left\langle \left[ \sum_{i=1}^{N} m_i |r_i - R|^2 \right] \right\rangle \quad (2)$$

where $R$ is the center of mass of the system, $r_i$ is the position vector of the $i$-th atom of mass $m_i$ and $M$ is the total mass of the system. According to our results, $R_g$ values of protonated G0-G3 PAMAM dendrimers at neutral pH are larger compared to those of non-protonated dendrimers due to the increased electrostatic repulsion between the terminal

**Table 2**
Radius of gyration $R_g$ (Å), aspect ratio ($I_x$ / $I_y$ and $I_x$ / $I_z$), and asphericity (δ) values obtained from 100 ns MD simulations for G0-G3 PAMAM and EOS-PAMAM systems at neutral and basic pH conditions.

| pH | System | $R_g$ (Å) | Aspect ratio | | Asphericity δ |
|---|---|---|---|---|---|
| | | | $I_x$ / $I_y$ | $I_x$ / $I_z$ | |
| Neutral | G0 | 6.1 ± 0.3 | 1.39 ± 0.21 | 2.00 ± 0.34 | 0.0406 ± 0.0160 |
| | G1 | 9.3 ± 0.5 | 1.27 ± 0.14 | 1.95 ± 0.36 | 0.0351 ± 0.0157 |
| | G2 | 12.6 ± 0.6 | 1.25 ± 0.12 | 1.91 ± 0.33 | 0.0330 ± 0.0141 |
| | G3 | 15.2 ± 0.6 | 1.28 ± 0.09 | 1.78 ± 0.24 | 0.0214 ± 0.0110 |
| Basic | G0 | 5.8 ± 0.2 | 1.43 ± 0.19 | 2.10 ± 0.36 | 0.0451 ± 0.0183 |
| | G1 | 8.4 ± 0.6 | 1.26 ± 0.14 | 2.07 ± 0.39 | 0.0402 ± 0.0166 |
| | G2 | 10.1 ± 0.6 | 1.21 ± 0.12 | 1.83 ± 0.40 | 0.0290 ± 0.0169 |
| | G3 | 13.1 ± 0.5 | 1.18 ± 0.09 | 1.66 ± 0.24 | 0.0271 ± 0.0102 |
| Neutral | G0-EOS | 6.1 ± 0.2 | 1.40 ± 0.20 | 1.95 ± 0.36 | 0.0382 ± 0.0179 |
| | G1-EOS | 9.0 ± 0.5 | 1.23 ± 0.13 | 1.97 ± 0.31 | 0.0354 ± 0.0176 |
| | G2-EOS | 12.2 ± 0.6 | 1.21 ± 0.11 | 1.83 ± 0.31 | 0.0291 ± 0.0137 |
| | G3-EOS | 14.7 ± 0.6 | 1.17 ± 0.07 | 1.86 ± 0.28 | 0.0303 ± 0.0130 |
| Basic | G0-EOS | 5.9 ± 0.2 | 1.44 ± 0.20 | 2.15 ± 0.37 | 0.0478 ± 0.0166 |
| | G1-EOS | 8.1 ± 0.6 | 1.21 ± 0.13 | 2.26 ± 0.56 | 0.0474 ± 0.0220 |
| | G2-EOS | 10.0 ± 0.4 | 1.18 ± 0.09 | 1.97 ± 0.33 | 0.0349 ± 0.0148 |
| | G3-EOS | 12.5 ± 0.2 | 1.12 ± 0.10 | 1.50 ± 0.23 | 0.0148 ± 0.0098 |

$-NH_3^+$ groups. This size expansion is more evident in higher generation dendrimers as reported earlier in the literature [18–20] Calculated $R_g$ values for PAMAM-G3 (15.2 Å and 13.1 Å in neutral and alkaline conditions, respectively) are in high agreement with theoretical estimations reported by Maiti et al. from MD simulations [19–21], and experimental measurements from small angle X-ray scattering (SAXS) [21,22], thus supporting the validity of our current MD approach. In the case of EOS-PAMAM systems, $R_g$ values reveal that EOS association in 1:1 ratio did not induce significant changes in the dendrimer size in both neutral and alkaline media.

Aspect ratios ($I_x/I_y$ and $I_x/I_z$) and asphericity (δ) were calculated to assess the shape anisotropy of PAMAM and EOS-PAMAM systems as a function of dendrimer generation and protonation state. The principal moments of inertia of the systems under study ($I_x$, $I_y$, and $I_z$) were obtained from the diagonalization of the gyration matrix and were employed to calculate the dimensionless aspect ratios $I_x/I_y$ and $I_x/I_z$ (Table 2). Calculated aspect ratios range between 1.1 and 2.1, and exhibit a progressive decrease in higher generation dendrimers, thus accounting for an increase in symmetry and spherical shape of PAMAM and EOS-PAMAM systems as the dendrimer generation becomes higher, in both neutral and alkaline conditions, with no significant shape changes upon EOS complexation.

The asphericity (δ) was calculated to provide more quantitative information about the shape of PAMAM and EOS-PAMAM systems. The asphericity (δ) is defined as

$$\delta = 1 - 3\left(\frac{\langle I_2 \rangle}{\langle I_1^2 \rangle}\right) \quad (3)$$

where $I_1$ and $I_2$ are defined as

$$I_1 = I_x + I_y + I_z \quad (4)$$

$$I_2 = I_x I_y + I_y I_z + I_z I_x \quad (5)$$

and values close to zero in δ account for a more spherical shape of the system under study. According to our results, PAMAM dendrimers and EOS-PAMAM systems acquire a more spherical shape as the dendrimer generation increases in both neutral and alkaline conditions. Nevertheless, all systems under study exhibited a high spherical symmetry, as revealed by the low values of δ, which are lower than 0.05.

The time evolution of the distance between the centers of mass of PAMAM and EOS was employed to further examine the process of dye complexation along the simulation run, as displayed in Fig. 3. At neutral pH, EOS molecules locate near to the dendrimers core during the first 10 ns of MD simulations, remaining stable at distances comprised between 6 and 10 Å along the trajectory. Under basic pH conditions, dye molecules took longer to locate inside the dendrimer structure, remaining at distances between 7 and 11 Å from the dendrimer core during the second half of the MD simulation run. These results suggest that protonated amino groups play a critical role on the host-guest interaction at neutral pH by attracting the anionic EOS molecules to the dendrimer surface over neutral amino groups at basic pH. Further information regarding the average location of EOS in PAMAM complexes was retrieved from radial distribution function analysis (Fig. S4), showing that neutral pH conditions enable a deeper penetration of the dye within PAMAM's structure as consequence of the expanded dendrimer structure in the protonated state. On the other hand, at basic pH the dendrimer structure becomes more compact, thus hindering the entrance of the EOS molecule to the innermost dendrimer cavities. This differential behavior is more evident in higher generation dendrimers, in which the size expansion due to protonation is more pronounced.

Representative equilibrated structures of EOS-PAMAM complexes at pH 7.0 and pH 10.0 obtained after 100 ns of NPT runs are displayed in Fig. 4. These snapshots show that complexed dyes molecules present a common association mode at both pH conditions, in which anionic ring is oriented towards the solvent, whereas the less polar xanthene moiety is oriented towards the innermost dendrimer cavities, with the exception of the EOS-PAMAM-G0 complex in which the dye is totally exposed to the solvent. To further explore the nature of the intermolecular interactions in the series of EOS-PAMAM complexes under study, NCI calculations were carried out using the last structure retrieved from MD trajectories. NCI is a valuable tool to study the favorable and unfavorable intermolecular interactions based on the peaks that appear in the reduced density gradient of a supramolecular system at low densities. [23] NCI results are customarily displayed with different colors, namely strongly attractive hydrogen bonding interactions are in blue, weakly attractive van der Waals interactions in green, and strongly repulsive steric clashes in red, as shown in Fig. 5. Details about NCI plots for the series of EOS-PAMAM complexes under study are provided as Supplementary material. According to NCI results, the EOS complexation within innermost dendrimer branches is mostly driven by van der Waals forces, whereas hydrogen bonds are responsible for the interaction with the surface amino groups of PAMAM. Regarding to hydrogen bonds, our results indicate that three main hydrogen bonds are observed within the series of EOS-PAMAM systems under study, namely (i) the interaction between the carboxylate group of EOS and the surface amino moieties of PAMAM, and (ii) the interaction between the carboxylate group and the NH amide moiety of the outermost branches of PAMAM, and (iii) the interaction between the phenolic oxygen atom

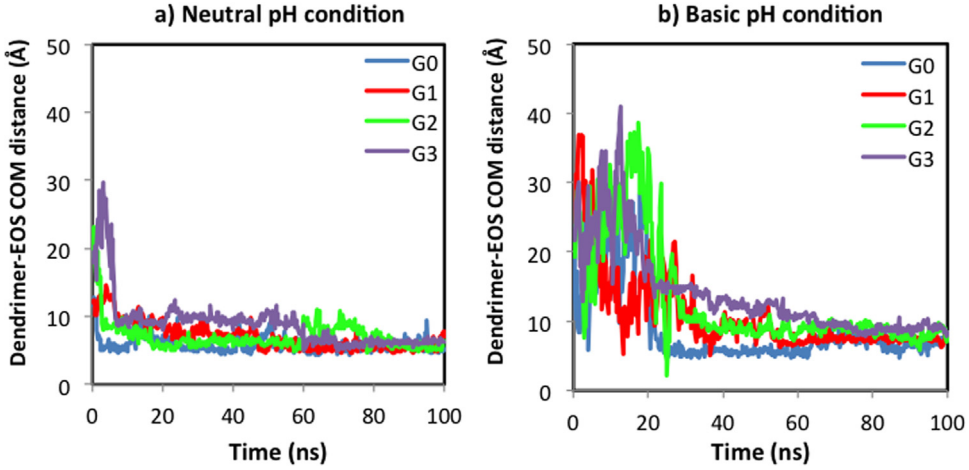


**Fig. 3.** Center-of-mass (COM) separation distance between PAMAM dendrimers (G0-G3) and EOS dye molecules along 100 ns of MD simulation run. a) Neutral pH condition, and b) basic pH conditions.

of the xanthene ring and the NH amide group of internal dendrimer branches, as illustrated in Fig. 5. These interactions have occupancies higher than 70% and are present in EOS-PAMAM systems at pH 7.0 and pH 10.0. Nevertheless, at neutral conditions, the corresponding occupancies increase as detailed in the Supplementary material section.

As a final theoretical approach to address the EOS-PAMAM

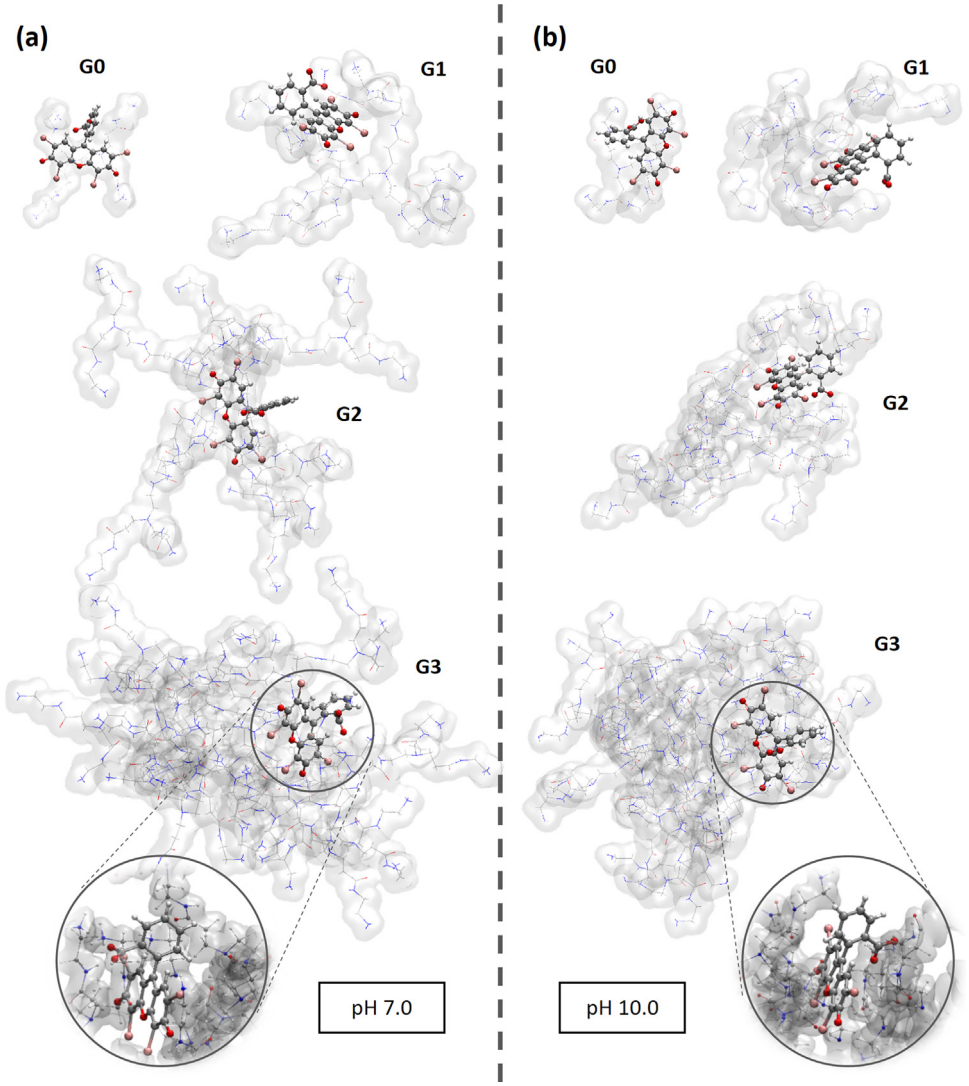


**Fig. 4.** Representative structures of EOS-PAMAM (G0-G3) complexes at neutral and basic pH conditions. Expanded images show the common association mode of EOS in the complexes.

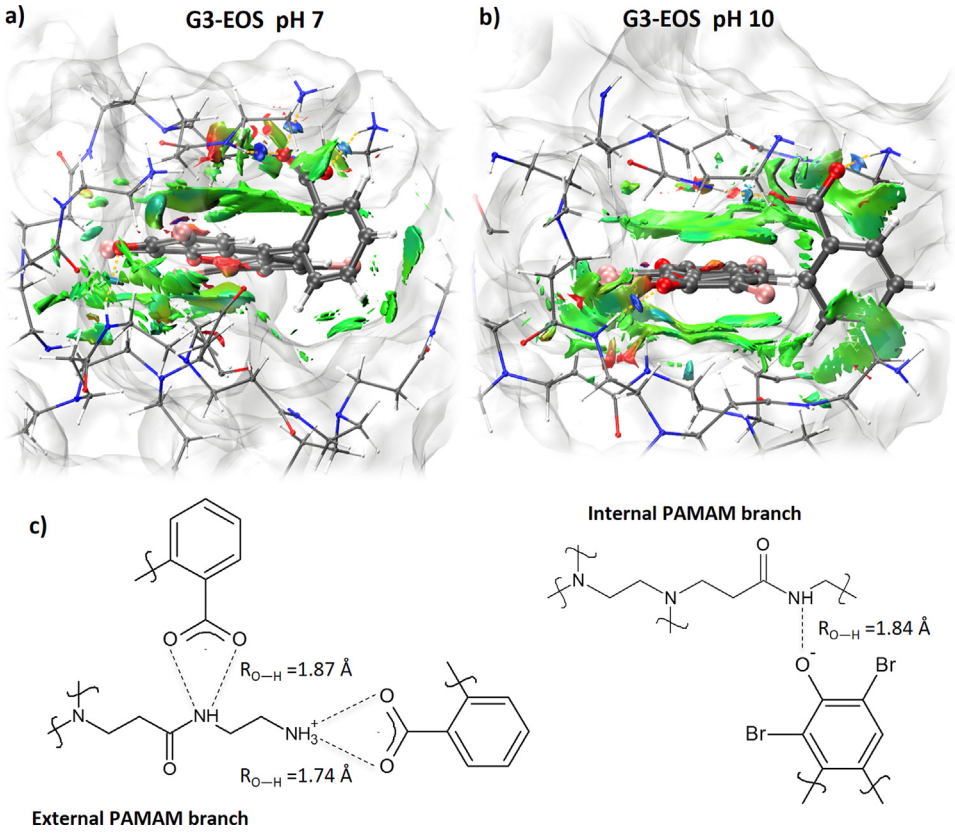


**Fig. 5.** (a)–(b) Representative NCI results for EOS-PAMAM systems at neutral and basic pH conditions. The isosurfaces are colored on a blue-red-green scale according to the values of $\lambda_{H,}$ ρ ranging from −0.10 to + 0.10 au. Blue indicates strong attractive interactions (hydrogen bonds), green indicates weak interactions (van der Waals), and red indicates strong repulsive interactions (steric clashes). (c) Hydrogen bonds in EOS-PAMAM systems. (For interpretation of the references to color in this figure legend, the reader is referred to the web version of this article.)

interaction, we carried out MM/PBSA binding free energy calculations using the following equation:

$$\Delta G_{bind} = G_{EOS-PAMAM} - (G_{PAMAM} + G_{EOS}) \quad (6)$$

The free energy $G$ corresponding to each molecule (i.e. EOS-PAMAM, PAMAM and EOS) was decomposed as follows:

$$G_{molecule} = E_{MM} + \Delta G_{solv} - TS \quad (7)$$

$$\Delta G_{solv} = \Delta G_{polar\,(PB\,or\,GB)} + \Delta G_{non-polar\,(SA)} \quad (8)$$

where the $E_{MM}$ is the sum of molecular mechanical gas–phase energies, $\Delta G_{solv}$ is the solvation free energy and -TS is the entropy contribution to the free energy. $\Delta G_{solv}$ is decomposed as the sum of polar and non-polar contributions. Polar contributions were estimated using the Poisson–Boltzmann (PB) implicit solvation model (ipb = 2), whereas the non-polar contribution was modeled as a sum of a cavity term and a dispersion term. Entropic contributions were ignored due to computational costs. MM/PBSA calculations were carried out using a single trajectory approach, in which the necessary ensembles for binding free energy calculations were retrieved from the last 50 ns of equilibrated MD runs. The strength of EOS-PAMAM interactions in the series of systems under study estimated from MM/PBSA calculations is displayed in Table 3. In agreement with experimental measurements, MM/PBSA binding free energy calculations indicate that EOS-PAMAM interactions are more favored under neutral pH conditions, and that the affinity of the dye towards complexation increases as the dendrimer generation becomes higher, thus supporting for the size-dependency of the supramolecular interaction between EOS and PAMAM. However, compared to experimental data, MM/PBSA calculations were found to overestimate the absolute values of binding free energies for EOS-PAMAM association, particularly under neutral pH conditions. The fact that $\Delta G_{calc}$ values are far from the experimental values in an absolute scale is a well-known issue and has been extensively reported in the literature [24,25]. This can be attributed to the enlargement of the relative contribution of the electrostatic and the polar solvation terms to the binding free energies in highly charged systems. Regarding to alkaline media, MM/PBSA calculations were in closer quantitative agreement with experimental results. At basic pH, the surface amino groups of PAMAM remain neutral, thus reducing the overestimation of the electrostatic contributions to the binding free energy. Nevertheless, besides predicting binding free energies in a quantitative agreement, the main goal of MM/PBSA calculations is to correctly rank the binding free energies in a series of related systems, which was successfully

**Table 3**
MM/GBSA binding energy components for PAMAM-EOS complexes at neutral and basic pH condition. All energies were calculate from the last 50 ns of simulation and are presented in kcal $mol^{-1}$.

| pH | System | $\Delta G_{vdW}$ (kcal $mol^{-1}$) | $\Delta G_{elec}$ (kcal $mol^{-1}$) | $\Delta G_{solv}$ (kcal $mol^{-1}$) | $\Delta G_{bind}$ (kcal $mol^{-1}$) |
|---|---|---|---|---|---|
| Neutral | G0-EOS | −17.2 | −376.9 | 383.4 | −10.7 ± 0.4 |
| | G1-EOS | −29.3 | −549.4 | 566.7 | −12.0 ± 0.3 |
| | G2-EOS | −37.9 | −843.0 | 865.5 | −15.4 ± 0.4 |
| | G3-EOY | −46.2 | −1328.3 | 1356.6 | −17.9 ± 0.4 |
| Basic | G0-EOS | −15.7 | −23.3 | 37.1 | −1.9 ± 0.4 |
| | G1-EOS | −18.8 | −25.9 | 42.1 | −2.7 ± 0.3 |
| | G2-EOS | −28.5 | −49.2 | 73.2 | −4.6 ± 0.3 |
| | G3-EOY | −42.8 | −92.1 | 128.0 | −6.9 ± 0.5 |

accomplished in this work for EOS-PAMAM systems at neutral and basic pH conditions. To get deeper insight about the relative contribution of different driving forces to the stability of EOS-PAMAM complexes, MM/GBSA binding free energy values were decomposed in van der Waals, electrostatic, and solvation energy contributions, as detailed in Table 3. These results indicated that both the electrostatic and the van der Waals terms for the EOS-PAMAM interaction increase under neutral pH conditions. This enhancement is partially compensated by the less favorable solvation term of charged systems at neutral pH. Nevertheless, the overall energetic effect supports for the stabilization of EOS-PAMAM complexes at pH 7.0 over pH 10.0 in high agreement with our experimental results.

A further analysis of MM/PBSA data (Fig. S9) reveals that MM/PBSA predictions show a very good linear correlation with experimental binding free energies at neutral pH ($r^2$ = 0.98), whereas at alkaline conditions the linear dependence between theoretical and experimental data was partially lost ($r^2$ = 0.90). The most significant deviation from linearity was observed for the EOS-PAMAM-G3 system, which is the largest neutral system under study. In this case, MM/PBSA calculations overestimate the binding strength in almost 1.3 kcal/mol, which is in the range of acceptable errors for MM/PBSA calculations [24,25]. Summarizing, the aforementioned provide reliable evidence about the good performance of the MM/PBSA approach to estimate ligand-binding affinities in supramolecular systems where dendrimers act as host macromolecules.

## 4. Conclusion

The supramolecular interaction between the EOS dye and low generation PAMAM G0-G3 dendrimers was studied using absorption spectroscopy experiments and MD simulations. Our results revealed that EOS-PAMAM interactions are strongly modulated by the pH of the medium being favored at neutral conditions (pH 7.0). Theoretical models are consistent with experimental findings and suggest a deeper, and faster penetration of the drug at neutral pH, and an increased affinity towards complexation as the dendrimer generation increases. Our current approach provides evidences of the valuable potential of using computational modelling to increase understanding about the molecular features responsible for supramolecular complexation phenomena involving PAMAM dendrimers as host molecules.

## Acknowledgement

Authors thank FONDECYT Grant number 1160060, Postdoctoral FONDECYT Grant 3160378. MZ thanks CONICYT doctoral fellowship number 21140192. Financial support from CONICET (PIP 2015-11220150100687CO) and Universidad Nacional de Río Cuarto is gratefully acknowledged.

## Appendix A. Supplementary material

Details of the simulated systems, radial distribution functions, and linearized absorbance data is provided as supporting information.

Supplementary data associated with this article can be found in the online version at doi:10.1016/j.jlumin.2018.03.068.

## References

[1] T. Hirano, K. Kikuchi, Y. Urano, T. Higuchi, T. Nagano, Highly zinc-selective fluorescent sensor molecules suitable for biological applications, J. Am. Chem. Soc. 122 (2000) 12399–12400.
[2] M.E. Martinez-Perez, A.D. Hughes, S.A. Thom, A.A. Bharath, K.H. Parker, Segmentation of blood vessels from red-free and fluorescein retinal images, Med. Image Anal. 11 (2007) 47–61.
[3] M. Sibrian-Vazquez, J.O. Escobedo, M. Lowry, F.R. Fronczek, R.M. Strongin, Field effects induce bathochromic shifts in xanthene dyes, J. Am. Chem. Soc. 134 (2012) 10502–10508.
[4] C. Thivierge, J.Y. Han, R.M. Jenkins, K. Burgess, Fluorescent proton sensors based on energy transfer, J. Org. Chem. 76 (2011) 5219–5228.
[5] J.R. Kim, S. Michielsen, Photodynamic antifungal activities of nanostructured fabrics grafted with rose bengal and phloxine B against Aspergillus fumigatus, J. Appl. Polym. Sci. 132 (2015).
[6] D.P. Hari, B. Konig, Synthetic applications of eosin Y in photoredox catalysis, Chem. Commun. 50 (2014) 6688–6699.
[7] E.M. Arbeloa, C.M. Previtali, S.G. Bertolotti, Photochemical study of Eosin-Y with PAMAM dendrimers in aqueous solution, J. Lumin. 180 (2016) 369–375.
[8] E.M. Arbeloa, C.M. Previtali, S.G. Bertolotti, Study of the Eosin-Y/PAMAM interactions in alkaline aqueous solution, J. Lumin. 172 (2016) 92–98.
[9] R. Esfand, D.A. Tomalia, Poly(amidoamine) (PAMAM) dendrimers: from biomimicry to drug delivery and biomedical applications, Drug Discov. Today 6 (2001) 427–436.
[10] D. Cakara, J. Kleimann, M. Borkovec, Microscopic protonation equilibria of poly (amidoamine) dendrimers from macroscopic titrations, Macromolecules 36 (2003) 4201–4207.
[11] K. Kaastrup, H.D. Sikes, Investigation of dendrimers functionalized with eosin as macrophotoinitiators for polymerization-based signal amplification reactions, RSC Adv. 5 (2015) 15652–15659.
[12] V. Maingi, V. Jain, P.V. Bharatam, P.K. Maiti, Dendrimer building toolkit: model building and characterization of various dendrimer architectures, J. Comput. Chem. 33 (2012) 1997–2011.
[13] J.M. Wang, R.M. Wolf, J.W. Caldwell, P.A. Kollman, D.A. Case, Development and testing of a general amber force field, J. Comput. Chem. 25 (2004) 1157–1174.
[14] M.J. Frisch, G.W. Trucks, H.B. Schlegel, G.E. Scuseria, M.A. Robb, J.R. Cheeseman, G. Scalmani, V. Barone, B. Mennucci, G.A. Petersson, H. Nakatsuji, M. Caricato, X. Li, H.P. Hratchian, A.F. Izmaylov, J. Bloino, G. Zheng, J.L. Sonnenberg, M. Hada, M. Ehara, K. Toyota, R. Fukuda, J. Hasegawa, M. Ishida, T. Nakajima, Y. Honda, O. Kitao, H. Nakai, T. Vreven, J.A. Montgomery, J.E. Peralta, F. Ogliaro, M. Bearpark, J.J. Heyd, E. Brothers, K.N. Kudin, V.N. Staroverov, R. Kobayashi, J. Normand, K. Raghavachari, A. Rendell, J.C. Burant, S.S. Iyengar, J. Tomasi, M. Cossi, N. Rega, J. M. Millam, M. Klene, J.E. Knox, J.B. Cross, V. Bakken, C. Adamo, J. Jaramillo, R. Gomperts, R.E. Stratmann, O. Yazyev, A.J. Austin, R. Cammi, C. Pomelli, J.W. Ochterski, R.L. Martin, K. Morokuma, V.G. Zakrzewski, G.A. Voth, P. Salvador, J.J. Dannenberg, S. Dapprich, A.D. Daniels, Farkas, J.B. Foresman, J.V. Ortiz, J. Cioslowski, D.J. Fox, Wallingford CT, 2009.
[15] V.R. Batistela, D.S. Pellosi, F.D. de Souza, W.F. da Costa, S.M.D. Santin, V.R. de Souza, W. Caetano, H.P.M. de Oliveira, I.S. Scarminio, N. Hioka, pK(a) determinations of xanthene derivates in aqueous solutions by multivariate analysis applied to UV-vis spectrophotometric data, Spectrochim. Acta Part Mol. Biomol. Spectrosc. 79 (2011) 889–897.
[16] T. Darden, D. York, L. Pedersen, Particle mesh ewald – an n.log(n) method for ewald sums in large systems, J. Chem. Phys. 98 (1993) 10089–10092.
[17] J.-P. Ryckaert, G. Ciccotti, H.J.C. Berendsen, Numerical integration of the cartesian equations of motion of a system with constraints: molecular dynamics of n-alkanes, J. Comput. Phys. 23 (1977) 327–341.
[18] L. Porcar, K. Hong, P.D. Butler, K.W. Herwig, G.S. Smith, Y. Liu, W.-R. Chen, Intramolecular structural change of PAMAM dendrimers in aqueous solutions revealed by small-angle neutron scattering, J. Phys. Chem. B 114 (2010) 1751–1756.
[19] P.K. Maiti, T. Cagin, S.T. Lin, W.A. Goddard, Effect of solvent and pH on the structure of PAMAM dendrimers, Macromolecules 38 (2005) 979–991.
[20] P.K. Maiti, T. Cagin, G.F. Wang, W.A. Goddard, Structure of PAMAM dendrimers: generations 1 through 11, Macromolecules 37 (2004) 6236–6254.
[21] P.K. Maiti, B. Bagchi, Diffusion of flexible, charged, nanoscopic molecules in solution: size and pH dependence for PAMAM dendrimer, J. Chem. Phys. 131 (2009).
[22] T.J. Prosa, B.J. Bauer, E.J. Amis, From stars to spheres: a SAXS analysis of dilute dendrimer solutions, Macromolecules 34 (2001) 4897–4906.
[23] J. Contreras-Garcia, E.R. Johnson, S. Keinan, R. Chaudret, J.P. Piquemal, D.N. Beratan, W.T. Yang, NCIPLOT: a program for plotting noncovalent interaction regions, J. Chem. Theory Comput. 7 (2011) 625–632.
[24] G. Rastelli, A. Del Rio, G. Degliesposti, M. Sgobba, Fast and accurate predictions of binding free energies using MM-PBSA and MM-GBSA, J. Comput. Chem. 31 (2010) 797–810.
[25] T.J. Hou, J.M. Wang, Y.Y. Li, W. Wang, Assessing the performance of the MM/PBSA and mm/gbsa methods. 1. The accuracy of binding free energy calculations based on molecular dynamics simulations, J. Chem. Inf. Model. 51 (2011) 69–82.